Soft Matter

RSC Publishing

PAPER

View Article Online
View Journal | View Issue

The dominant role of the solvent–water interface in water droplet templating of polymers†

Cite this: *Soft Matter*, 2013, **9**, 7960

Ronan Daly,‡*[a] John E. Sader[ab] and John J. Boland[a]

We investigate the formation of microstructured polymer networks known as Breath Figure templated structures created by the presence of water vapour over evaporating polymer solutions. We use a highly controlled experimental approach to examine this dynamic and non-equilibrium process to uniquely compare pure solvent systems with polymer solutions and demonstrate using a combination of optical microscopy, focused ion-beam milling and SEM analysis that the porous polymer microstructure is completely controlled by the interfacial forces that exist between the water droplet and the solvent until a final drying dilation of the imprints. Water droplet contact angles are the same in the presence or absence of polymer and are independent of size for droplets above 5 μm. The polymer acts a spectator that serves to trap water droplets present at the air interface, and to transfer their shape into the polymer film. For the smallest pores, however, there are unexpected variations in the contact angle with pore size that are consistent with a possible contribution from line tension at these smaller dimensions.

Received 24th May 2013
Accepted 8th July 2013

DOI: 10.1039/c3sm51452h

www.rsc.org/softmatter

Introduction

Polymers are widely recognised as critically important enabling materials with applications in many technologies. Although early applications exploited bulk properties such as elasticity, it was recognised early on that polymers provide a unique opportunity to control the microstructure of materials. Microstructuring of polymers has in turn opened up important applications in foams, photonics and pharmaceutical delivery technologies. Microstructuring is most frequently accomplished by exploiting miscibility and interfacial energy differences between components in polymer blends. Self-organisation in di- and tri-block copolymers offers a dramatic demonstration of this phenomenon and can lead to microstructures that are only limited by the sizes of the individual blocks (10 nm or less). Patterned and porous materials in 2- and 3-D can then be produced by elimination of one or more blocks.

A particularly rich and interesting example of polymeric film microstructure control is the three component system examined in this work involving a polymer dissolved in a volatile organic solvent that is exposed to water vapour over the surface of the polymer solution. An example of the resulting ordered microstructure from this three-component system is shown in Fig. 1a. The structures are believed to be the imprints of condensed water droplets;[1] the product of a system of evaporative cooling of the solvent, water vapour condensation into droplets on the surface and the increasing relative polymer concentration as the solvent leaves to finally capture the droplet

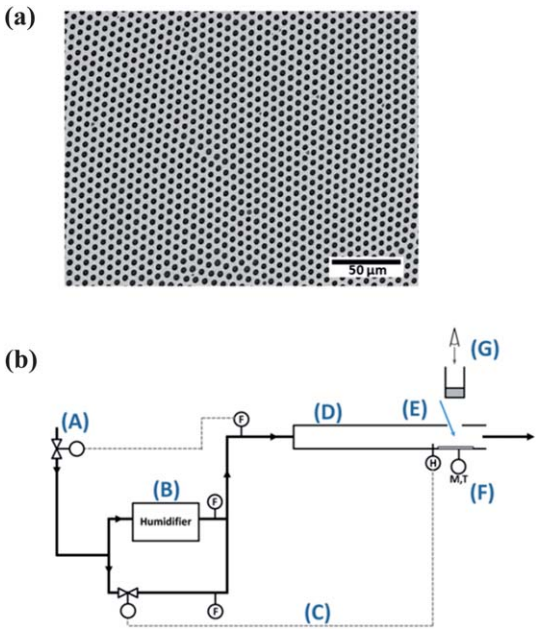

Fig. 1 Water droplets can be used to template an entangled polymer film formed through solvent evaporation. As shown in (a) the ordered structure of the imprints is formed due to ordering of the water droplets. The controlled system used to form these structures is illustrated in (b).

[a]*School of Chemistry and Centre for Research on Adaptive Nanostructures and Nanodevices (CRANN), Trinity College Dublin, Dublin 2, Ireland*

[b]*Department of Mathematics and Statistics, University of Melbourne, Melbourne, Australia*

† Electronic supplementary information (ESI) available. See DOI: 10.1039/c3sm51452h

‡ Current address: Department of Engineering, University of Cambridge, UK. E-mail: rd439@cam.ac.uk; Tel: +44 (0) 1223 766141

structure. Despite the ease of fabrication of these so-called Breath Figures (BF) and the wide range of potential applications,[2] the mechanism of imprint formation is still not well understood.[3] Although the requirement for water vapour is an almost universally accepted part of the mechanism,[4–7] several reports have suggested the water is initially present in the solvent[8] or that pore formation is the result of solvent boiling.[9]

Where it is agreed that the imprints are created by water droplets, the position of these water droplets has been described as being above the solution–air interface,[10] stabilised at the interface[11] or just below the interface with a final step involving the opening of the imprinted pores as the solvent recedes.[12] Divergent views on the positioning of the droplets have also led to diverse mechanisms to account for droplet stabilisation and non-coalescence and to explain how droplets become ordered to create the observed BFs.[6,10,12–15]

Here in this paper, we attempt to elucidate the mechanism by separating the behaviour of a pure solvent–water system from that of the final polymer containing system. Critically, we demonstrate the contact angles at which droplets are stable at the solution–air interface remain unchanged from pure solvent systems to viscous polymer solutions. Contrary to suggestions in the literature, while the polymer is essential to capturing the final ordered structure, it in fact plays a minimal role in the microscale droplet stabilisation mechanism and in defining where the droplets sit in relation to the solvent–air surface. We show that the water droplets are almost entirely submerged at the solution interface for the duration of the process and the final microstructure is a replica of this system, stabilised by a complex surface tension balance governed by the properties of the solvent; the polymer does not exert an observable effect on the three-phase stability problem. Additionally, we show that for the case of nanoscale droplets and imprint formation, there is some evidence that the three-phase line tension may play a role.

Materials and methods

The solvents used within this study were (i) chloroform for spectroscopy, Uvasol® supplied by Merck, (ii) toluene puriss., absolute, over molecular sieve ($H_2O \leq 0.005\%$), $\geq$99.7% (GC) supplied by Sigma Aldrich and (iii) butyl acetate anhydrous, $\geq$99% supplied by Sigma Aldrich. Water used within the study was both de-ionised and filtered. The experimental arrangement used in this work is shown in Fig. 1b. The flow of carrier gas (99.999% nitrogen) is controlled by a flow controller/meter arrangement (A) while the relative humidity (RH) is controlled by passing part of this stream through a humidifier (B) and monitored by a hygrometer at the point of use (C). The carrier gas is not expected to be a significant component as it is inert, clean and also dry. The growth chamber (D) includes a port (E) for dosing the polymer solution onto a glass cover slip. The mass and temperature changes during the formation process can be recorded by the *in situ* mass balance and ultra-fine thermocouple incorporated into the chamber (F). The entire process can be monitored in real time by optical microscopy (G) to provide a direct measure of the evolution of the droplet contact angles.

Results and discussion

Using three solvents, butyl acetate, toluene and chloroform we first demonstrated[16] by optical microscopy that water droplet raft formation across the surface of the pure organic solvents can only be achieved when a stream of carrier gas is entrained with humidity. Micro-droplets of water at the solvent–air interface respond to changes in the local relative humidity and grow or shrink as the water vapour–liquid-equilibrium is altered.[16] Butyl acetate is used here and in previous work[16] as it is less volatile and has fewer toxicity issues compared with other organic solvents and so allowed close examination of droplet condensation, droplet evaporation and stability at the solvent interface. Two solvents, common in the Breath Figure literature, namely toluene and chloroform are used predominantly in this work to make the polymer solutions. The formation of rafts of droplets again occurs at the polymer solution surface and again the droplets grow or shrink depending on the relative humidity. Video evidence, as provided in the ESI,† shows that once water droplets have formed and packed across the polymer solution surface, a subsequent reduction in relative humidity leads to evaporation of the water droplets and in fact leads to complete recovery of the surface and the absence of any microstructure in the polymeric matrix. This has been demonstrated in a more simple form by manually dosing microdroplets of water onto a butyl acetate surface and maintaining a low relative humidity, as shown in Fig. 2a–c.

The droplets have a bulls-eye appearance with the outer diameter reflecting the overall size of the droplet and the inner diameter the three phase contact line or crown where the droplet protrudes above the polymer solution. Note in the system shown in Fig. 2c the droplet shrinks over time in these low humidity conditions. We now turn to the structure of individual water droplets at the surface of both pure solvents and polymer solutions. Using the method of Mingins and Scheludko[17] we measured the contact angle of water droplets as determined by the ratio of the diameter of the exposed crown to that of the submerged droplet as described previously for pure solvent–water systems.[16] For each of the pure solvents studied in the previous work the contact angles were found to be independent of the droplet size.

In all cases, whether dosed manually or by condensation, we observe water droplets remain almost completely submerged in the solvent–air or polymer solution–air interface, as shown in Fig. 2a–c and illustrated in Fig. 2d. In our highly controlled experiments using thin solution layers for droplet raft formation, we did not observe water droplets being removed from the surface into the bulk solution. The rafts remained highly stable at the solution–air interface. This is true for both toluene and chloroform systems where the densities are less than and greater than water respectively. This supports the view that multi-layered structures of imprints are not due to the differing solvent densities as at these length-scales we are far below the associated bond number and gravity effects can be neglected.[18] Multi-layered structures were only observed in our work with the addition of significant quantities of surfactants or some nanomaterials, where the effect on droplet stability is extreme.

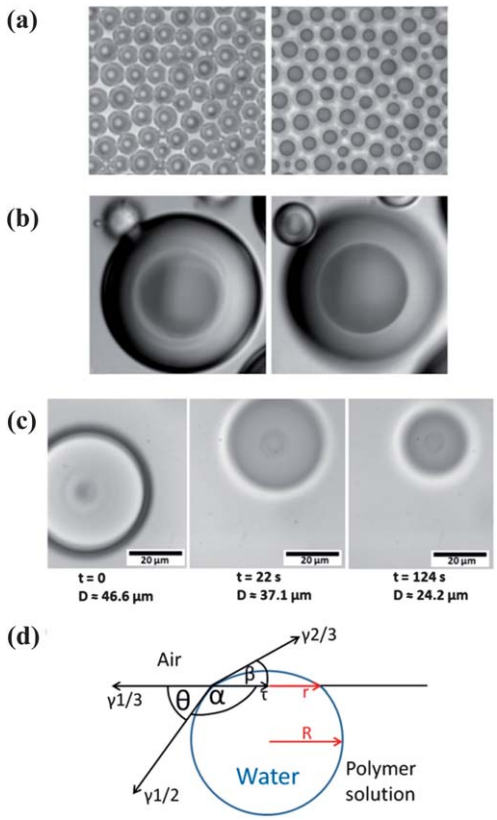

Fig. 2 Using the method described for pure solvent systems,[16] a system of $3\%_{w/w}$ dicarboxy-terminated polystyrene (DCPS) in chloroform can be templated from condensed water droplets while measuring the three phase contact radius, *r*, and the larger submerged radius, *R*. The focal plane can be changed to focus on the two or three phase radius as shown for (a) with shrinking of a water droplet at a butyl acetate–air interface, recorded over 124 seconds at ambient relative humidity or (b) for single droplets over short time periods. The same technique is applied in (c) to an array of water droplets in polymer solution. The geometry defined in (d) allows the use of the method defined by Mingins and Scheludko[17] to determine contact angle, α.

(a)

Solvent	Contact angle, α (Degrees)
Chloroform	145.7 ± 3.5
Chloroform + DCPS	142.7 ± 2.7
Toluene	170.0 ± 2.4
Toluene + DCPS	167.0 ± 1.5

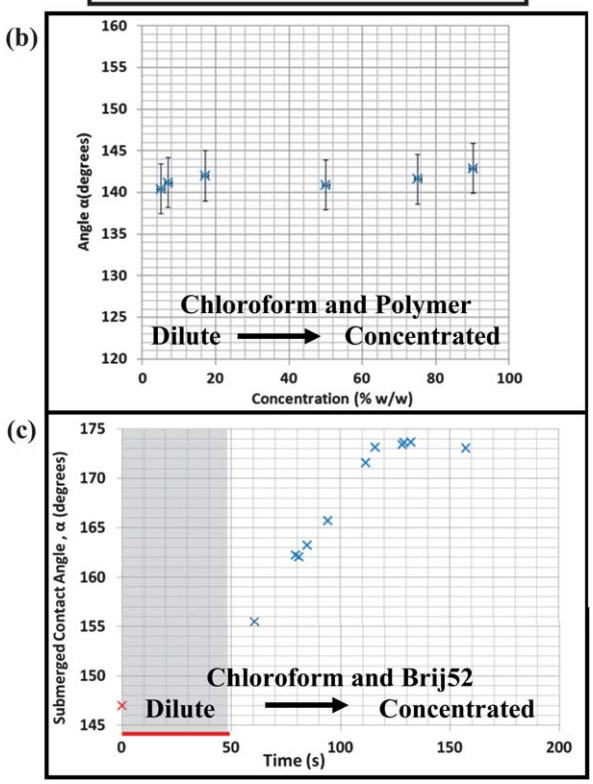

Fig. 3 (a) Comparison of submerged water droplet contact angles measured at chloroform and toluene interfaces, both with and without polymer. (b) It is seen for a set of measurements during one run that there is no significant change in the contact angle as the polymer concentration increases due to evaporation of chloroform. (c) The change in contact angle of water droplets in chloroform is shown by optical microscopy as the surfactant Brij52 migrates to the solvent interfaces. The first point indicated in red is the pure solvent value, which is expected to be the initial point. Due to the complexity of the measurement, the first minute cannot be captured and this is indicated with a red line.

This is explored in a series of follow-up experiments to be reported. Our controlled experimental approach is observed to reduce the surface currents significantly compared with standard humidity chambers or thicker solution films. Because of this, the rafts of water droplets pack in a two-dimensional hcp arrangement in the presence or absence of polymer and significant coalescence does not occur in either case.

Using chloroform and toluene as two separate test systems we added $3\%_{w/w}$ of dicarboxy-terminated polystyrene and repeated the droplet raft formation and contact angle measurement experiments. In both cases, contact angles for the water droplets at the polymer solution–air interface were not significantly different to those of pure solvent systems (see Fig. 3a). Using the experimental setup in Fig. 1b it is possible to monitor water droplets at the polymer solution–air interface and record the solvent loss due to evaporation. Thus starting from the $3\%_{w/w}$ polymer solution it is possible to estimate the increasing polymer concentration (as solvent evaporates) and to measure the corresponding changes in the droplet contact angles. We note that this estimate represents a lower bound since the actual polymer concentration is not likely to be homogeneous in the *z* direction during evaporation and there may in fact be a gradient with an elevated concentration nearer to the top and a lower concentration nearer to the substrate at the early stages of this experiment. Fig. 3b shows that for chloroform, the contact angle is relatively constant during the evaporation process and remains so up until pore formation, when the water is removed. A similar behaviour is also noted for the toluene based system until there is sudden change due to a dilation of the pore opening due to drying, as discussed below.

The results in Fig. 3b and c, in combination with our earlier results on pure solvent summarised in Fig. 3a, suggest that the mechanism of droplet stabilization is controlled by the solvent and most importantly that the polymer does not significantly modify the surface tension at the air–polymer solution

interface. To test this hypothesis and to demonstrate the sensitivity of our technique, we performed measurements in which we included small quantities ($0.06\%_{w/w}$) of the surfactant Brij52 (polyoxyethylene 2 cetyl ether) in the casting polymeric solution. Fig. 3c shows that there is a dramatic increase in the submerged water droplet contact angle (142 to 175°) with time, consistent with a lowering of the solvent–water and polymer solution–air interfaces with surfactant migration.

The rate of surfactant migration to the solvent–water interface is sufficiently slow as to provide observable changes in the droplet contact angle (see Fig. 3c). As this is not the case with the polymer solution system over a significantly longer duration, it is likely that a different mode of action is occurring. The polymer contains carboxylic acid end groups and is believed to form larger aggregates in solution.[6] It is also suggested that these precipitate at the water interface to stabilise the droplets. For the contact angle to be maintained with the addition of polymer, this may indicate the polymer is not precipitating at the water interface until very late in the process, when the highly viscous nature of the solution has already stabilised the shape. Alternatively the precipitation occurs but does not modify the low interfacial tension significantly. While the mechanism is still not conclusive, it is clear from the statistically robust measurements that the result is a very close templating of the droplets at contact angles associated with the pure solvent system.

The question now is to what extent does the droplet shape, contact angles and positioning at the interface control the final porous microstructure after the water droplet finally evaporates. To address this we used optical microscopy to follow the pore formation process from droplet nucleation through to solvent evaporation and drying. It was noticed that there is a sudden dilation and increase of the imprinted pore opening as the polymer sets the droplets and the water evaporates in the final stage of the drying process. This was more noticeable in the case of toluene and is included in the ESI.† We have analyzed the resulting pore structures by careful low-energy focused ion beam (FIB) cross-sectioning, followed by scanning electron microscopy (SEM).

An example is shown in Fig. 4, which reveals a cross section of two spherical pores formed using dicarboxy-terminated polystyrene and chloroform. The central feature in Fig. 4 is the remnants of an adjacent pore in the hexagonally close-packed arrangement and not a submerged pore. A more delicate form of the FIB-SEM analysis was performed for pores of different sizes and compared with the optical images and contact angles parameters determined for the same systems using optical methods. There are several important observations. First, for both toluene and chloroform-based samples the contact angles determined from the polymer replica of the water droplets using SEM are once again constant for different size pore but consistently lower than those found optically (see Fig. 5a and b). It is believed that this apparent difference in contact angles and the dilation in the pore opening, which can be directly seen under a microscope, is due to a drying phenomenon associated with the recession or collapse of the extremely thin polymer film that had previously been present at the water–air interface (illustrated in Fig. 5c). This phenomenon is more pronounced in the case of toluene compared to chloroform, since the contact angle is extremely high for the former and hence the polymer film around the pore opening is particularly thin.

These results suggest that the detailed pore microstructure is controlled by the solvent choice, and the structure of the pores

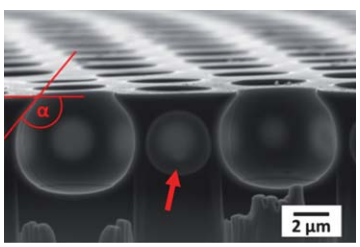

Fig. 4 Focused ion beam milling is used to form a cross section of the droplet imprints. Imprints are formed from a solution of dicarboxy terminated polystyrene in chloroform. Note that the central feature indicated with an arrow is the side of an adjacent pore and not a submerged pore.

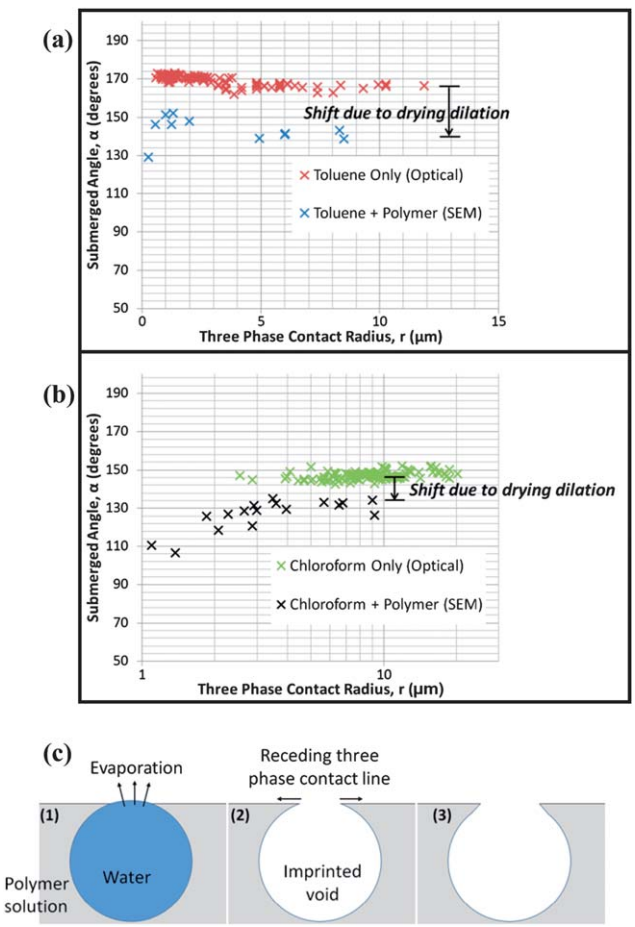

Fig. 5 The difference is noted between contact angles observed optically during formation and recorded by scanning electron microscopy (SEM) post formation. The observed difference in contact angle is shown for (a) a toluene system, and (b) for a chloroform system for different size pores. A change in the contact angle with pore radius, *r*, is observed for chloroform based polymer imprinting. The observed dilation of the three phase contact line is illustrated in (c).

produced is entirely predictable once the drying-induced recession of the imprint opening is taken into account. A second immediate observation is that in all cases the polymer droplet replicas are spherical in shape. This is important since it conclusively demonstrates that the drop sizes are well below their capillary lengths and hence buoyancy or gravity have no role in stabilizing or controlling the position of the water droplets at the interface or in the mechanism of pore formation.[2,19]

A particular advantage of FIB-SEM analysis of the post pore formation is the ability to study pores of all sizes, even those that are too small for optical methods. In contrast to the behaviour of large diameter pores, the contact angle is seen to be less predictable when the three phase contact radius, r, is of the order 0.3–5 μm. As shown in Fig. 5a and b, while toluene-based samples appear to maintain a constant contact angle, chloroform-based samples show a significant decrease in the contact angle for small imprinted pores. This is highlighted in Fig. 6 where we have placed below each imprint cross section the extracted internal curvature profile in black and a comparison curve in red (suitably re-scaled) representing the expected constant contact angle. While it is noted and shown that the original contact angles of stable droplets are modified with drying, this change is seen to be size independent until we consider the chloroform-based system. Evidently, in the case of chloroform there is potentially a new mechanism at play that causes the actual contact angle to decrease as the droplet size and the imprint decrease in size.

While there may be additional drying effects that act on smaller imprints, this does not explain the additional influence on chloroform-based samples. Of the solvents studied, chloroform leads to the smallest imprint contact angle and hence the thickest polymer film around the opening and so is the least sensitive to drying effects. At these small dimensions, however, discussion in the literature has pointed to the possible role of line tension at the three-phase contact line[16] and so we have tried to incorporate to test if this is feasible. Given that the internal microstructure is close to spherical, we can use the balance of interfacial forces discussed by Pujado and Scriven[20] and shown in eqn (1) to examine the possible combined roles of line and surface tension. Details of the assumptions this approach entails are discussed in the ESI† of the work looking at stability mechanisms of droplets at pure solvent–air interfaces.[16]

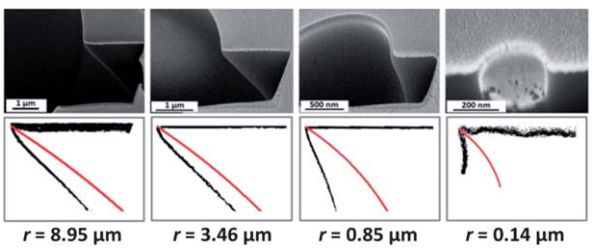

Fig. 6 The difference between the predicted contact angle (in red) and the observed contact angle extracted from the image (black) deviates more significantly for small imprints when examining a chloroform system.

$$\alpha = \arccos\left(\frac{{\gamma_{12}}^2 - {\gamma_{23}}^2 + \left(\gamma_{13} - \frac{\tau}{r}\right)^2}{2\gamma_{12}\left(\gamma_{13} - \frac{\tau}{R}\right)}\right) \quad (1)$$

Using standard literature values for the solvent–air and solvent–water surface tensions, the data in Fig. 5b can be modelled using eqn (1), where α is the submerged contact angle defined in Fig. 2d, γ_{12} is the water–solvent interfacial tension, γ_{13} is the polymer solution–air surface tension, γ_{23} is the water–air surface tension, r represents the three phase contact radius, R is the larger submerged radius and τ is the line tension.

The fitting parameters are τ and γ_{23}. Surface tension at the air–water interface, γ_{23}, deviates from literature values due to solvent migration, which is known to be a key factor for droplet stabilization.[16] The fit to eqn (1) shown in Fig. 7 closely matches the data and returns a line tension of $\tau = -8$ nN and a modified water–air surface tension $\gamma_{23} = 53$ mN m^{-1}. We note that γ_{23} is significantly reduced from the literature value of 72.8 mN m^{-1}, which is consistent with the presence of solvent over the air–water interface.[16] For all other required surface and interfacial tensions, we relied upon previously reported values[16] where it was confirmed that neither the use of nitrogen nor a high relative humidity lead to significant changes. Careful cleaning of substrates and use of only high purity solvents allowed us to minimize any deviation from these reported values. The value for line tension we find here is small and negative, in the range of that predicted in the literature[21] and is indicative of a small force working to expand the three phase contact region and to stabilise the droplet at the air interface. However, a more detailed study of nanoscale water droplets and pores is required before the contribution of line tension can be decisively confirmed. However, clearly the controversy regarding the reconciliation between theoretically predicted and experimentally noted values for line tension will need to be considered in further detail.

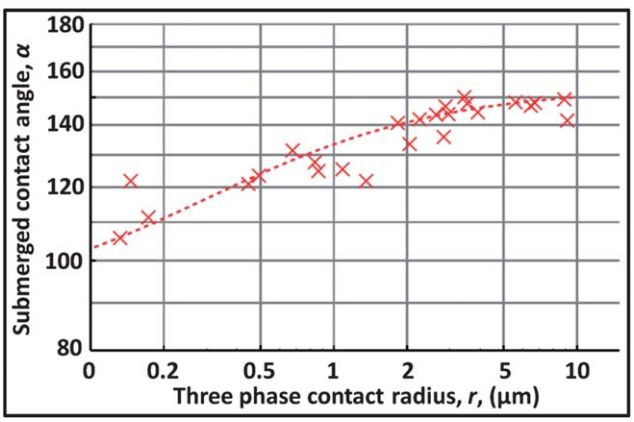

Fig. 7 A fit with eqn (1) for the data in Fig. 5b showing the change in contact angle with three phase contact radius for chloroform-based polymer imprints. Results obtained from a series of imprints of different size. These were examined by focused ion beam cross-sectioning and fit fitting parameters of $\tau = -8 \times 10^{-9}$ N and $\gamma_{23} = 53$ mN m^{-1}.

Conclusions

In conclusion we have shown that the porous polymer microstructure is completely controlled by the properties of the water–solvent system, and that the polymer is a spectator that only serves to capture the shape of the water droplet that exists at the air interface. While the polymer is observed to provide additional stability to the droplets against coalescence in previous reports[12] our experimental set-up was designed so that stable droplet rafts can be tracked for pure solvents also and to directly compare behaviour with polymer-containing solutions. The final imprint shape in the polymer matrix is controlled by interfacial forces that exist between the water droplet and the solvent, including a significant lowering of the air–water interfacial tension, possibly due to the presence of a solvent film. The fidelity of the transfer of shape from the droplet to the polymer is excellent, and the only variations that arise are due to shrinkage of the thin polymer wedge at the openings of the pores. For the smallest pores, however, there are unexpected variations in the contact angle with pore size that are consistent with a possible contribution from line tension at these smaller dimensions.

Acknowledgements

The financial support of Science Foundation Ireland (Grant No. 06/IN.1/I106) and the Australian Research Council grants scheme are gratefully acknowledged.

Notes and references

1 B. François, O. Pitois and J. François, *Adv. Mater.*, 1995, **7**, 1041–1044.
2 U. H. F. Bunz, *Adv. Mater.*, 2006, **18**, 973–989.
3 E. Bormashenko, S. Balter and D. Aurbach, *Macromol. Chem. Phys.*, 2012, **213**, 1742–1747.
4 G. Widawski, M. Rawiso and B. François, *Nature*, 1994, **369**, 387–389.
5 O. Pitois and B. Francois, *Colloid Polym. Sci.*, 1999, **277**, 574–578.
6 M. H. Stenzel, C. Barner-Kowollik and T. P. Davis, *J. Polym. Sci., Part A: Polym. Chem.*, 2006, **44**, 2363–2375.
7 M. S. Barrow, R. L. Jones, J. O. Park, M. Srinivasarao, P. R. Williams and C. J. Wright, *Spectroscopy*, 2004, **18**, 577–585.
8 M. S. Park and J. L. Kim, *Langmuir*, 2004, **20**, 5347–5352.
9 E. Bormashenko, R. Pogreb, O. Stanevsky, Y. Bormashenko and O. Gendelman, *Mater. Lett.*, 2005, **59**, 3553–3557.
10 M. Srinivasarao, D. Collings, A. Philips and S. Patel, *Science*, 2001, **292**, 79–83.
11 A. Steyer, P. Guenoun and D. Beysens, *Phys. Rev. E: Stat. Phys., Plasmas, Fluids, Relat. Interdiscip. Top.*, 1993, **48**, 428–431.
12 O. Pitois and B. Francois, *Eur. Phys. J. B*, 1999, **8**, 225–231.
13 N. Maruyama, T. Koito, J. Nishida, T. Sawadaishi, X. Cieren, K. Ijiro, O. Karthaus and M. Shimomura, *Thin Solid Films*, 1998, **327–329**, 854–856.
14 L. A. Connal, R. Vestberg, C. J. Hawker and G. G. Qiao, *Adv. Funct. Mater.*, 2008, **18**, 3706–3714.
15 L. Billon, M. Manguian, V. Pellerin, M. Joubert, O. Eterradossi and H. Garay, *Macromolecules*, 2009, **42**, 345–356.
16 R. Daly, J. E. Sader and J. J. Boland, *Langmuir*, 2012, **28**, 13218–13223.
17 J. Mingins and A. Scheludko, *J. Chem. Soc., Faraday Trans. 1*, 1979, **75**, 1–6.
18 L. Li, Y. Zhong, J. Li, J. Gong, Y. Ben, J. Xu, X. Chen and Z. Mad, *J. Colloid Interface Sci.*, 2010, **342**, 192–197.
19 A. Bolognesi, C. Mercogliano and S. Yunus, *Langmuir*, 2005, **21**, 3480–3485.
20 P. R. Pujado and L. E. Scriven, *J. Colloid Interface Sci.*, 1972, **40**, 82–98.
21 A. Amirfazli and A. W. Neumann, *Adv. Colloid Interface Sci.*, 2004, **110**, 121–141.